frontiers | Frontiers in Physics

TYPE Original Research
PUBLISHED 01 March 2023
DOI 10.3389/fphy.2023.1064601

OPEN ACCESS

EDITED BY
Maria Piarulli,
Washington University in St. Louis,
United States

REVIEWED BY
Heiko Hergert,
Michigan State University, United States
Praveen C Srivastava,
Indian Institute of Technology Roorkee,
India

*CORRESPONDENCE
K. S. Becker,
kbeck13@lsu.edu

SPECIALTY SECTION
This article was submitted
to Nuclear Physics,
a section of the journal
Frontiers in Physics

RECEIVED 08 October 2022
ACCEPTED 13 January 2023
PUBLISHED 01 March 2023

CITATION
Becker KS, Launey KD, Ekström A and
Dytrych T (2023), *Ab initio* symmetry-
adapted emulator for studying emergent
collectivity and clustering in nuclei.
Front. Phys. 11:1064601.
doi: 10.3389/fphy.2023.1064601

Ab initio symmetry-adapted emulator for studying emergent collectivity and clustering in nuclei

K. S. Becker[1]*, K. D. Launey[1], A. Ekström[2] and T. Dytrych[1,3]

[1]Department of Physics and Astronomy, Louisiana State University, Baton Rouge, LA, United States, [2]Department of Physics, Chalmers University of Technology, Gothenburg, Sweden, [3]Nuclear Physics Institute, Academy of Sciences of the Czech Republic, Řež, Czech Republic

We discuss emulators from the *ab initio* symmetry-adapted no-core shell-model framework for studying the formation of alpha clustering and collective properties without effective charges. We present a new type of an emulator, one that utilizes the eigenvector continuation technique but is based on the use of symplectic symmetry considerations. This is achieved by using physically relevant degrees of freedom, namely, the symmetry-adapted basis, which exploits the almost perfect symplectic symmetry in nuclei. Specifically, we study excitation energies, point-proton root-mean-square radii, along with electric quadrupole moments and transitions for ^{6}Li and ^{12}C. We show that the set of parameterizations of the chiral potential used to train the emulators has no significant effect on predictions of dominant nuclear features, such as shape and the associated symplectic symmetry, along with cluster formation, but slightly varies details that affect collective quadrupole moments, asymptotic normalization coefficients, and alpha partial widths up to a factor of two. This makes these types of emulators important for further constraining the nuclear force for high-precision nuclear structure and reaction observables.

KEYWORDS

***ab initio* symmetry-adapted no-core shell model, nuclear collectivity, nuclear clustering, eigenvector continuation, emulators, 6Li, 12C**

Introduction

Ab initio approaches to nuclear structure and reactions (for an overview, see Ref. [1]) aim to provide accurate predictions based on few-nucleon forces, such as the ones derived from chiral effective field theory (EFT) [for a review, see e.g. Ref. [2] and references therein]. To achieve this, it is imperative to utilize high-precision nuclear forces that accurately describe nuclear correlations, from short- to long-range correlations, as well as to quantify uncertainties that arise from the nuclear force and the controlled approximations in solving the many-body Schrödinger equation [3]. Such developments use statistical tools, including, for example, Bayesian analysis [4], global sensitivity methods [5], and uncertainty estimates based on regression [6, 7], that sometimes require a large number of computationally intensive calculations which often poses a challenge.

In this paper, we seek to overcome some of these difficulties by combining the symmetry-adapted no-core shell model (SA-NCSM) framework [8–10] with the methodology of eigenvector continuation (EVC) [5, 11, 12]. The SA-NCSM uses a physically relevant basis that, in manageable model spaces, achieves descriptions of light to medium-mass nuclei, including challenging nuclear features, such as collectivity, clustering, and related continuum effects. Similarly, EVC further reduces the sizes of Hamiltonian matrices by mapping them onto much smaller matrices referred to as emulators, low-dimensional manifolds built upon a set of characteristic solutions to the many-body Schrödinger equation. The proposed

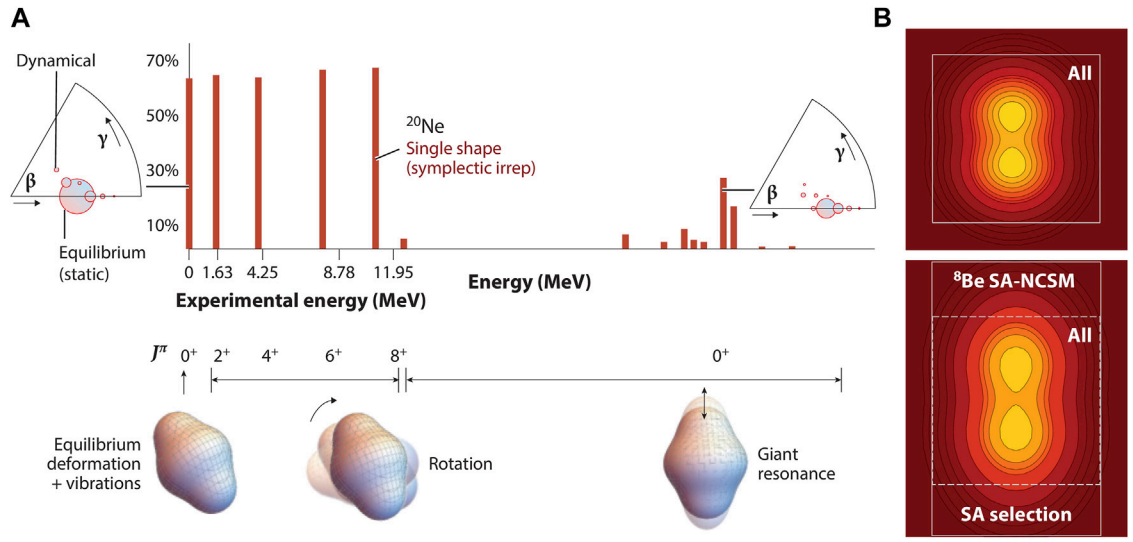

FIGURE 1
(A) Emergent symplectic symmetry in nuclei: Contribution of the most dominant shape to the 0^+ ground state of ^{20}Ne and its rotational band (2^+, 4^+, 6^+, and 8^+), as well as to excited 0^+ states, pointing to a fragmented giant monopole resonance [8]; for selected states, the deformation distribution within a shape is shown in terms of the shape parameters, the average deformation β and triaxiality angle γ (based on *ab initio* SA-NCSM calculations with NNLO$_{\rm opt}$ in a model space of 11 HO shells with $\hbar\Omega$ = 15 MeV inter-shell distance). **(B)** Schematic illustration of the SA concept shown for ^{8}Be: a smaller model space (square) includes all possible shapes (labeled as "All") and yields spatially compressed wave functions (top); a larger model space (rectangle in lower panel) accommodates, in a well prescribed way, spatially extended modes ("SA selection") that are neglected in smaller model spaces. Figure from Ref. [9] under the terms of its CC BY license.

symmetry-adapted eigenvector continuation (SA-EVC) method opens the door to calculations up through the medium-mass region and studies of collective and clustering nuclear features that otherwise might be computationally infeasible.

With a view toward inferring new knowledge of the nuclear forces relevant to structure and reaction observables, we construct novel SA-EVC emulators to study collective and clustering nuclear properties in ^{6}Li and ^{12}C (an emulator for the ^{6}Li binding energy is validated in Ref. [13]). Because this study focuses on the method validity, we utilize SA-NCSM calculations for a single harmonic oscillator (HO) strength $\hbar\Omega$, for which and for a specific parameterization of the chiral potential we show that the observables under consideration converge with the number of HO excitations, including point-proton root-mean-square (rms) radii and $E2$ transitions. The SA-NCSM utilizes a symplectic Sp(3,$\mathbb{R}$)-adapted basis and selected model spaces[1] that are significantly reduced in size due to symmetry considerations without sacrificing the physics of interest. Moreover, we show that the set of chiral potential parameterizations used to train the emulators has no significant effect on dominant nuclear features such as the nuclear shape (and associated symplectic symmetry) and cluster formation, making the SA model spaces highly suitable for this study. However, from one parameterization to another we find that probability amplitudes of wave functions and cluster peak distance vary slightly, affecting by a factor of two or less collective quadrupole moments, asymptotic normalization coefficients (ANCs), and alpha partial widths (which provide the probability for the alpha decay among all possible decays of a state). This suggests that these types of observables, and associated emulators, are important to inform and construct the nuclear forces for high-precision nuclear calculations.

Theoretical methods

Ab initio symmetry-adapted no-core shell model

Ab initio large-scale calculations [8, 9] have recently revealed a remarkably ubiquitous and almost perfect symmetry, the Sp(3,$\mathbb{R}$) symplectic symmetry, in nuclei that naturally emerges from first principles up through the calcium region (anticipated to hold even stronger in heavy nuclei [14]). Since this symmetry does not mix nuclear shapes, this novel nuclear feature provides important insight from first principles into the physics of nuclei and their low-lying excitations as dominated by only one or two collective shapes—equilibrium shapes with their vibrations—that rotate (Figure 1A).

The SA-NCSM theory [8, 10, 15] capitalizes on these findings and exploits the idea that the infinite Hilbert space can be equivalently spanned by "microscopic" nuclear shapes and their rotations [or symplectic irreducible representations (irreps), subspaces that preserve the symmetry], where "microscopic" refers to the fact that these configurations track with the position and momentum coordinates of each particle. A collective nuclear shape can be viewed as an equilibrium ("static") deformation and its vibrations ("dynamical" deformations) of the giant-resonance type, as illustrated in the β-γ plots of Figure 1A [8, 16]. A key ingredient of the SA concept is illustrated in Figure 1B, namely, while many shapes relevant to low-lying states are included in typical shell-model spaces (Figure 1B, top),

1 Throughout the paper, we will refer to the selected SA-NCSM model spaces as SA model spaces.

the vibrations of largely deformed equilibrium shapes and spatially extended modes like clustering often lie outside such spaces. The selected model space in the SA-NCSM remedies this, and includes, in a well prescribed way, those configurations. Note that this is critical for enhanced deformation, since spherical and less deformed shapes, including relevant single-particle effects, easily develop in comparatively small model-space sizes.

In this study, we utilize the *ab initio* SA-NCSM theory [8–10] that is based on the NCSM concept [17, 18] with nuclear interactions typically derived from the chiral EFT (e.g. [2, 19–23]). We use SA-NCSM model spaces, which are reorganized to a correlated basis that respects the shape-preserving Sp (3,$\mathbb{R}$) symmetry and its embedded symmetry, the deformation-related SU(3) [8–10]. We note that while the model utilizes symmetry groups to construct the basis and calculate matrix elements, descriptions are not limited *a priori* to any symmetry and can account for significant symmetry breaking.

The SA-NCSM is reviewed in Refs. [9, 10] and has been applied to light and medium-mass nuclei using SU(3)- and Sp(3,$\mathbb{R}$)-adapted bases. The many-nucleon basis states of the SA-NCSM are constructed using efficient group-theoretical algorithms and are labeled according to SU(3) × SU(2) by the proton, neutron and total intrinsic spins, S_p, S_n, and S, respectively, and $(\lambda_\omega\ \mu_\omega)$ quantum numbers with $\lambda_\omega = N_z - N_x$ and $\mu_\omega = N_x - N_y$, where $N_x + N_y + N_z = N_0 + N$, for a total of $N_0 + N$ HO quanta distributed in the x, y, and z directions[2]. Here, $N_0\hbar\Omega$ is the lowest total HO energy for all particles ("valence-shell configuration") and $N\hbar\Omega$ ($N \leq N_{\max}$) is the additional energy of all particle-hole excitations. Thus, for example, $(\lambda_\omega\ \mu_\omega) = (0\ 0)$, for which $N_x = N_y = N_z$, describes a spherical configuration, while N_z larger than $N_x = N_y$ ($\mu_\omega = 0$) indicates prolate deformation. In addition, a closed-shell configuration has (0 0). Indeed, spherical shapes, or no deformation, are a part of the SA basis. However, most nuclei—from light to heavy—are deformed in the *body-fixed* frame, which for 0^+ states appear spherical in the *laboratory* frame.

Furthermore, considering the embedding symmetry Sp(3,$\mathbb{R}$) ⊃SU(3), one can further organize SU(3) deformed configurations into subspaces that preserve Sp(3,$\mathbb{R}$) symmetry. Each of these subspaces (symplectic irrep, labeled by σ) is characterized by a given equilibrium shape, labeled by a single deformation $N_\sigma(\lambda_\sigma\ \mu_\sigma)$. For example, the symplectic irrep $N_\sigma(\lambda_\sigma\ \mu_\sigma) = 0(8\ 0)$ in ^{20}Ne consists of a prolate 0(8 0) equilibrium shape (static deformation) with $\lambda_\omega = 8$ and $\mu_\omega = 0$ in the valence-shell 0p-0h (0-particle-0-hole) subspace, along with many other SU(3) deformed configurations or dynamical deformation (vibrations), such as $N_\omega(\lambda_\omega\ \mu_\omega) = 2(10\ 0)$, 2(6 2), and 8 (16 0), which include particle-hole excitations of the equilibrium shape to higher shells [8, 14, 16]. These vibrations are multiples of $2\hbar\Omega$ 1p-1h excitations of the giant-resonance monopole and quadrupole types, that is, induced by the monopole $r^2 = \sum_{i=1}^{A} \vec{r}_i \cdot \vec{r}_i$ and quadrupole $Q_2 = \sqrt{16\pi/5}\sum_{i=1}^{A} r_i^2 Y_2(\hat{r}_i)$ operators, respectively (for further details, see Refs. [10, 24]).

An advantage of the SA-NCSM is that the SA model space can be down-selected from the corresponding ultra-large $N_{\max}$ complete model space to a subset of SA basis states that describe static and dynamical deformation, and within this SA model space the spurious center-of-mass motion can be factored out exactly [25, 26]. Another benefit is the use of group theory for constructing the basis and calculating matrix elements, including the Wigner-Eckart theorem, which allows for calculations with SU(3) reduced matrix elements that depend only on $(\lambda\ \mu)$, along with computationally efficacious group-theoretical algorithms and data structures, as detailed in Refs. [27–31]. A third advantage is that deformation and collectivity are examined and treated in the approach *without* the need for breaking and restoring rotational symmetry. The reason is that basis states utilize the $SU(3)_{(\lambda\ \mu)} \supset SO(3)_L$ reduction chain that has a good orbital angular momentum L, whereas all SU(3) reduced matrix elements can be calculated in the simpler canonical $SU(3)_{(\lambda\ \mu)} \supset SU(2)_I$ reduction chain (for details, see Refs. [32, 33]). The canonical reduction chain provides a natural reduction to the x and y degrees of freedom, it is simple to work with, and most importantly, provides a complete labeling of a basis state that includes the single-shell quadrupole moment eigenvalue that measures the deformation along the body-fixed symmetry z-axis [34]. SU(3) reduced matrix elements calculated within this scheme yield, in turn, matrix elements for the SA-NCSM basis by invoking the Wigner-Eckart theorem with the appropriate $SU(3)_{(\lambda\ \mu)} \supset SO(3)_L$ Clebsch-Gordan coefficients that are readily available [32].

We emphasize that all basis states are kept up to some $N_{\max}^{C}$, yielding results equivalent to the corresponding $N_{\max}^{C}$ NCSM calculations. Building upon this complete $N_{\max}^{C}$ model space, we expand the model space to $N_{\max}$ by adding selected basis states to include only the necessary vibrations of largely deformed equilibrium shapes that lie outside this $N_{\max}^{C}$ (such SA-NCSM model spaces are denoted as $\langle N_{\max}^{C}\rangle N_{\max}$).

Eigenvector continuation method in the symmetry-adapted framework

As introduced in Ref. [11], the EVC method utilizes the fact that if a Hamiltonian is a smooth function of some real-valued parameters, its eigenvectors will also be well-behaved functions of those parameters. In practice, this means that one can use a relatively small number of known wave functions to construct an accurate emulator well-approximated by a low-dimensional manifold, and with it accurately predict observables for an arbitrary chiral potential parameterization [12]. To compute these initial wave functions from first principles, it is advantageous to use SA model spaces that can accommodate deformation, including spatially expanded modes, as well as medium-mass regions.

An advantage of the EVC method is that solutions are achieved by diagonalizing matrices with sizes that are many orders of magnitude smaller than those used in exact calculations. This results in a drastically reduced computational time with practically no discrepancies from the exact results. EVC thus provides a means of generating large samples of nuclear observables from variations in the Hamiltonian parameters. This, in turn, makes computationally intensive statistical analyses, such as sensitivity studies [5, 12], possible. It also allows for a reduced computational load for quantifying uncertainties of *ab initio* predictions.

In this study, we construct emulators capable of probing collective and clustering features by employing the EVC method with SA model spaces. As illustrated in Table 1, the SA-NCSM reduces the sizes of Hamiltonian matrices by up to four orders of magnitude, or equivalently by more than 97%. The application of EVC to these SA spaces results in an additional reduction of up to 3 more orders of

2 We follow the notations of Ref. [15].

TABLE 1 Model space dimensions (labeled as "Dim"), excitation energy E_X, point-proton rms radius r_{rms}, electric quadrupole moment Q, and B ($E2\uparrow$) transition strengths from the ground state (g.s.) to the first excited state of ^{6}Li and ^{12}C, calculated with NNLO$_{opt}$ and $\hbar\Omega$ = 15 MeV in SA and complete model spaces. $\langle 2_{All}\rangle 8_{13}$ denotes an N_{max} = 2 model space with all symplectic irreps (complete), 13 Sp (3,$\mathbb{R}$) irreps of which extend to N_{max} = 8; 6_3 denotes 3 Sp (3,$\mathbb{R}$) irreps up to N_{max} = 6.

Nucleus	J^π	SA						Complete					
		N_{max}	Dim	E_X [MeV]	r_{rms} [fm]	Q [e fm^2]	B ($E2\uparrow$) [e^2 fm^4]	N_{max}	Dim	E_X [MeV]	r_{rms} [fm]	Q [e fm^2]	B ($E2\uparrow$) [e^2 fm^4]
^{6}Li	$1^+_{g.s.}$	$\langle 2_{All}\rangle 8_{13}$	4,898	–	2.20	−0.25	9.75	8	2×10^5	–	2.22	−0.028	10.04
^{6}Li	3^+_1	$\langle 2_{All}\rangle 8_{13}$	9,108	2.20	2.20	−4.12	–	8	3×10^5	2.65	2.22	−4.21	–
^{12}C	$0^+_{g.s.}$	6_3	552	–	2.41	0	35.31	6	1×10^6	–	2.43	0	35.22
^{12}C	2^+_1	6_3	238	5.73	2.41	+5.67	–	6	5×10^6	3.38	2.43	+5.56	–

magnitude, or as much as 99%. In this combined framework, the final size of the resulting matrices are as much as 10^{-5} times smaller than they would be in the corresponding N_{max} complete spaces. As the first step, we consider a chiral EFT nucleon-nucleon (NN) interaction truncated at next-to-next-to-leading order (NNLO), which depends on 14 low-energy constants (LECs). It turns out that we can write the chiral Hamiltonian as $H(\vec{c}) = \sum_{i=0}^{14} c_i h_i$, where $\vec{c}$ is a vector representing a unique combination of the LECs, h_i are the constituent chiral potentials, h_0 is the LEC-independent part of the chiral potential plus relative kinetic energy and the Coulomb interaction, and $c_0 = 1$.

A state $|\psi(\vec{c})\rangle$ can be well-approximated as a linear combination of known "training" wave functions $\sum_j^{N_T} \alpha_j(\vec{c})|\psi(\vec{c_T}_j)\rangle$, where each $|\psi(\vec{c_T}_j)\rangle$ in this study is the lowest-energy eigenvector of $H(\vec{c_T}_j)$ for a given J^π, $\vec{c_T}$ corresponds to a training point in the LEC parameter space, and N_T is the number of training points. The chiral Hamiltonian matrices h_i are constructed in the representation of the training wave functions. These $N_T \times N_T$ matrices are used to emulate the wave function for any set of LECs $\vec{c}$ by solving the Schrödinger equation for the unknown $\alpha_j(\vec{c})$ as a generalized eigenvalue problem that uses the norm matrix for the training wave functions, $M_{ij} = \langle\psi(\vec{c_T}_i)|\psi(\vec{c_T}_j)\rangle$.

The new features here are that we generate the emulator for the electric quadrupole moment Q by constructing the Q matrix in the representation of the training eigenvectors (as done for rms radii in Ref. [5]), and that these are calculated using SA model spaces. The quadrupole moment is then approximated by computing $\langle\psi(\vec{c})|Q|\psi(\vec{c})\rangle = \sum_{ij}\alpha_i(\vec{c})\alpha_j(\vec{c})\langle\psi(\vec{c_T}_i)|Q|\psi(\vec{c_T}_j)\rangle$.

Results and discussions

The results presented in this paper use the SA-NCSM in an Sp(3,$\mathbb{R}$) basis with an NN chiral potential up to NNLO as used in [21]. The consistent treatment of NN and three-nucleon (3N) forces at this order is feasible but outside the scope of the present study, which aims to show the validity of the SA-EVC method. We also include the outcomes for a specific NN parameterization, NNLO$_{opt}$ [21], for which the 3N forces have been shown to contribute minimally to the 3- and 4-nucleon binding energy [21]. Furthermore, the NNLO$_{opt}$ NN potential has been found to reproduce various observables, including the ^{4}He electric dipole polarizability [35]; the challenging analyzing power for elastic proton scattering on ^{4}He, ^{12}C, and ^{16}O [36]; neutron-deuteron scattering cross-sections [37]; along with B (E2) transition strengths for ^{21}Mg and ^{21}F [38] in the SA-NCSM without effective charges.

For the EVC calculations, we use N_T = 32 training points within the 14-dimensional parameter space for NNLO. We restrict the ranges of the LECs to lie within ±10% of their values for NNLO$_{opt}$ [21] and adopt the regularization for NNLO$_{opt}$. We sample training points using a randomly seeded latin hypercube design, and validate the emulators for 256 points that are different from the training points but within the same range of the LECs.

The SA-EVC results start with SA model spaces that are reduced by three to four orders of magnitude compared to the corresponding N_{max} complete model space (or, equivalently, NCSM calculations), as outlined in Table 1. Moreover, the associated observables are in good agreement for SA and complete model spaces, with differences that are typically comparable to differences resulting from varying $\hbar\Omega$ (see Ref. [8], supplemental material). Specifically, for the example of NNLO$_{opt}$, we report in Table 1 excitation energies, point-proton rms radii, electric quadrupole moments, and B ($E2\uparrow$) transition strengths between the two lowest energy states of ^{6}Li and ^{12}C. We also show that for the SA spaces used to train the emulators all of the above observables are converged with N_{max} (Figure 2).

Thus, for example, as shown in Table 1, collectivity-driven observables agree within 0.3%–2.9%, and radii agree at the sub-percent level. The largest deviation is observed for the ^{6}Li 1^+ quadrupole moment, however, it is important that its sign and very small magnitude are reproduced in both calculations. Furthermore, such differences are expected to decrease in richer model spaces; indeed, in a series of benchmark studies for light nuclei such as ^{4}He, ^{6}Li, ^{12}C, and ^{16}O (reviewed in Ref. [9]), we have shown that the SA-NCSM uses significantly smaller model spaces in comparison to the corresponding large complete N_{max} model spaces without compromising the accuracy for various observables (including electron scattering form factors [39] and sum rules [35]), as well as for effective inter-cluster potentials [31]. Reference [9] has also shown that for light nuclei, the SA-NCSM is in reasonable agreement with other *ab initio* approaches, such as hyperspherical harmonics [40, 41], the NCSM [17, 18], and quantum Monte Carlo [42].

Collectivity and clustering of training wave functions

An important feature of the training wave functions is that the dominant deformed configurations, or the SU(3) content of the states

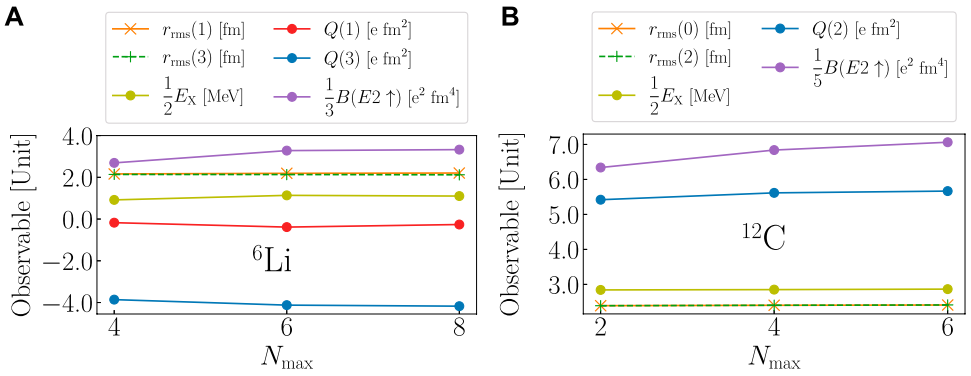

FIGURE 2
Convergence with $N_{\rm max}$ of the quadrupole moments $Q(J)$, point-proton rms radii $r_{rms}(J)$, excitation energies E_X, and B ($E2\uparrow$) transition strengths for the two lowest-lying states in **(A)** ^{6}Li and **(B)** ^{12}C. Observables are computed with the NNLO$_{\rm opt}$ parameterization for $\hbar\Omega$ = 15 MeV in SA model spaces reported in Table 1.

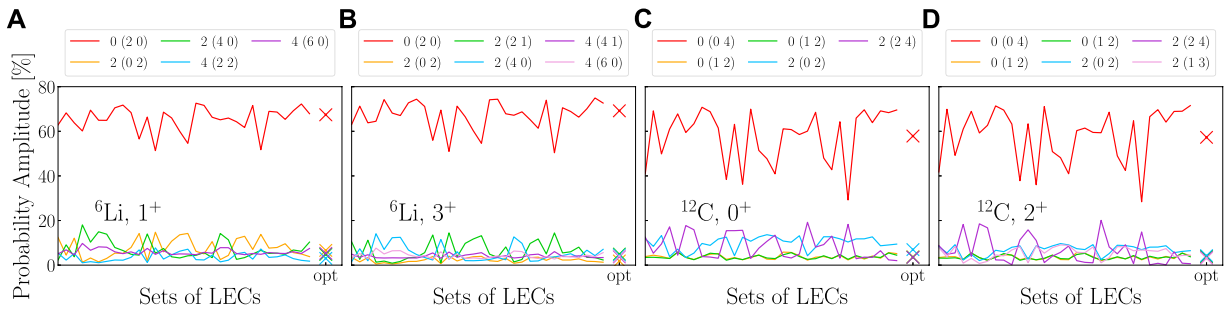

FIGURE 3
The largest SU (3) probability amplitudes (solid lines) as a function of emulator training LECs sets for **(A)** ^{6}Li 1$^+$ ground state and **(B)** ^{6}Li 3^+_1 state in $N_{\rm max}$ = $\langle 2_{\rm All}\rangle 8_{13}$ model space [all SU(3) states have $\{S_p, S_n, S\} = \{\frac{1}{2}, \frac{1}{2}, 1\}$], as well as for **(C)** ^{12}C 0$^+$ ground state and **(D)** ^{12}C 2^+_1 state in $N_{\rm max} = 6_3$ [all SU(3) states have $\{S_p, S_n, S\}$ = {0, 0, 0} except for 0 (1 2) with $\{S_p, S_n, S\}$ = {0, 1, 1} (orange) and {1, 0, 1} (green)]. Results are also shown for the NNLO$_{\rm opt}$ parameterization in the corresponding $N_{\rm max}$ complete model space (labeled as "opt").

under consideration, remain practically the same for all of the training wave functions (Figure 3). In addition, the SU(3) content agrees with the probabilities obtained with NNLO$_{\rm opt}$ in the corresponding $N_{\rm max}$ complete model space, also shown in Figure 3. This ensures that the same static and dynamical deformed modes govern the physics for all LECs sets under considerations, thereby justifying the use of the same SA selection for all the training wave functions.

Specifically, we find that one SU(3) irrep dominates the dynamics of each state at the 50%–60% level, with several additional configurations each contributing from 1% to 20% depending on the LECs set. Moreover, when the basis states are further organized into Sp(3,$\mathbb{R}$) irreps, we find that a single symplectic irrep—which contains the dominant SU(3) configurations—contributes at practically the same level from one training wave function to another. For example, the (2 0) symplectic irrep in ^{6}Li accounts for 83%–88% of each 1$^+$ training wave function, whereas the (2 0) contributes at the 85%–88% level in the case of the 3$^+$, out of thirteen available different irreps. Similarly, the probability of the (0 4) irrep in each of the ^{12}C training ground states is between 80%–88%, and between 82%–94% for the first 2$^+$ states. This is a strong indicator that the emulators are trained on wave functions that retain the symmetry-preserving and symmetry-breaking patterns that are observed in nuclei [8] and that the SA model spaces used in this study are sufficient to capture nuclear collectivity. Indeed, the fact that the Sp(3,$\mathbb{R}$) symmetry remains a near perfect symmetry for each of the training wave functions, retaining the same shape from one wave function to another, further supports the use of SA selections in the EVC method, or otherwise, the SA model spaces would need to be re-examined.

Another important feature of the training wave functions is that cluster formation is largely unaffected by the choice of interaction parameters. To study this, we project the ^{6}Li states onto the $\alpha + d$ system, following Ref. [43]: we use a ground state for each cluster that is renormalized to the most dominant SU(3) configuration, and we adopt R-matrix theory to match the amplitude of the cluster wave function and its derivative to those of the exact Coulomb eigenfunctions at large distances. We note that we are primarily interested in the effect of the LECs on the correlations in the training wave functions; hence, we fix the threshold energy to the experimental one. For the $^3S_1$ partial wave, we observe about 20%

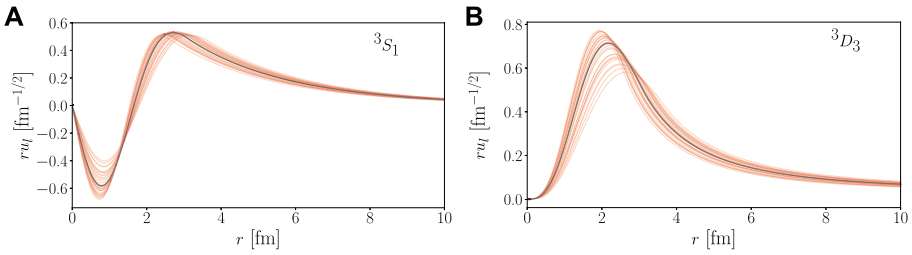

FIGURE 4
$\alpha + d$ **(A)** $^3S_1$-wave and **(B)** $^3D_3$-wave as functions of the relative distance r, computed from the ^{6}Li training wave functions for SA model spaces reported in Table 1. The spread of the curves is given by the $\pm$ 10% variation in the LECs. The case for NNLO$_{\text{opt}}$ is shown in black.

variations in the calculated asymptotic normalization coefficients (C_0 = 1.45–2.07 fm$^{-1/2}$) around their average value and 10% variations in the spectroscopic factor, namely, SF = 0.75–0.90 (Figure 4A). This tracks with the ±10% variation in the LECs. For comparison, the NNLO$_{\text{opt}}$ ANC for this particular channel is C_0 = 1.77 fm$^{-1/2}$ with SF = 0.87. Interestingly, the height of the second peak, which is located near the nuclear surface and informs the probability of cluster formation, remains fixed for all the parameterizations and coincides with the one for the NNLO$_{\text{opt}}$ case, only its position slightly varies with the LECs.

While the $^3D_3$ spectroscopic factors (SF = 0.73–0.92, with 0.90 for NNLO$_{\text{opt}}$) vary approximately at the 15% level (Figure 4B), which is practically the same as for the $^3S_1$ partial wave, α widths of the 3^+ state range from Γ_α = 6.34 keV–14.05 keV, which is about ±40% from Γ_α = 9.81 keV calculated for this particular channel with NNLO$_{\text{opt}}$ (similarly to the ANCs, we use the experimental threshold energy). We note that the NNLO$_{\text{opt}}$ values for C_0 and Γ_α are reported for a single channel without taking excitations of the clusters into account (e.g., see Ref. [44]) and should not be compared directly to experiment. Of particular interest for this study is that the LECs sets induce a change in both the location and magnitude of the peak, to which the probability for alpha decay is typically sensitive to.

To summarize, the behavior of the surface peaks in both channels and the nuclear shapes of the 1^+ and 3^+ states in ^{6}Li (as well as the shapes of the 0^+ and 2^+ states in ^{12}C) are relatively consistent. This suggests that the terms of the nuclear potential that are independent of the LECs, including parts of the long-range interaction, are largely responsible for cluster formation, along with the development of the nuclear shape [equivalently, almost perfect Sp(3,$\mathbb{R}$) symmetry]. In contrast, the LECs, which capture the unresolved short-ranged interactions between nucleons, fine-tune collective and clustering features, and affect the associated observables by only a factor, namely, 1.4 for the $1^+_{\text{g.s.}}$ ANCs, 2.2 for the 3^+_1 alpha width, and 1.4 for the 3^+_1 quadrupole moment in ^{6}Li. Similarly, the quadrupole moment for the 2^+_1 in ^{12}C is affected by a factor of 2.1. While the clustering features are explored in this study for the training points only, the SA-EVC approach—the validation of which is discussed next—enables uncertainty quantification of such collective and reaction observables if the probability distributions for the LECs are available.

Validation of the symmetry-adapted eigenvector continuation

To validate the SA-EVC approach, we show that for the quadrupole moments of the ^{6}Li 1^+ ground state and first excited 3^+ state, as well as for the 3^+ excitation energy, the emulators provide very accurate results compared to the exact outcomes (Figure 5). The average relative errors over all 256 validation LECs sets are respectively 6.91 × 10^{-2}, 7.70 × 10^{-4}, and 1.20 × 10^{-4}. It is clear that any deviations of the emulators from the expected values are negligible, especially considering that, as mentioned above, the SA selection reduces the Hamiltonian dimension by more than 97%, and the EVC projection by an additional 99% or more.

It is worth noting that the average error for the ground state quadrupole moment is two orders of magnitude larger than that of the 3^+ state. We note that $Q(1^+)$ of ^{6}Li is very similar in nature to the deuteron quadrupole moment. The extremely small value in both nuclei results from a small mixing of an L = 2 component into the ground state of ^{6}Li (and of the deuteron), which is not collective in essence like, e.g., the quadrupole moments of the 3^+ state in ^{6}Li or the 2^+ state in ^{12}C (discussed below). Indeed, the results of Figure 5A reflect the high sensitivity of the underlying NN interaction (and likely 3N forces [46]) to the L = 2 mixing in the ground state wave function.

Similar to ^{6}Li, the SA-EVC emulated 2^+_1 quadrupole moment and excitation energy for ^{12}C are in very close agreement to the exact results (Figure 6). Namely, the average relative errors are given by 1.02 × 10^{-4} and 6.72 × 10^{-5}, respectively. Compared to the average errors reported above for the 3^+_1 quadrupole moment and excitation energy for ^{6}Li, we find eight and two times improvement in the emulator's predictions for ^{12}C, respectively. The reason is likely related to the much smaller SA selection in ^{12}C and the stronger collective nature observed in the low-lying states of ^{12}C. Specifically, in ^{6}Li the SA-EVC uses thousands of basis states, whereas in ^{12}C only hundreds of basis states (see Table 1). We therefore expect the mixing of configurations to exert a more noticeable effect on ^{6}Li than on ^{12}C. The result is that the eigenvectors of ^{12}C vary in fewer directions than those of ^{6}Li, suggesting that more training points for ^{6}Li may be beneficial to improve errors. While this warrants further study, this speaks to an advantage of merging the SA and EVC frameworks.

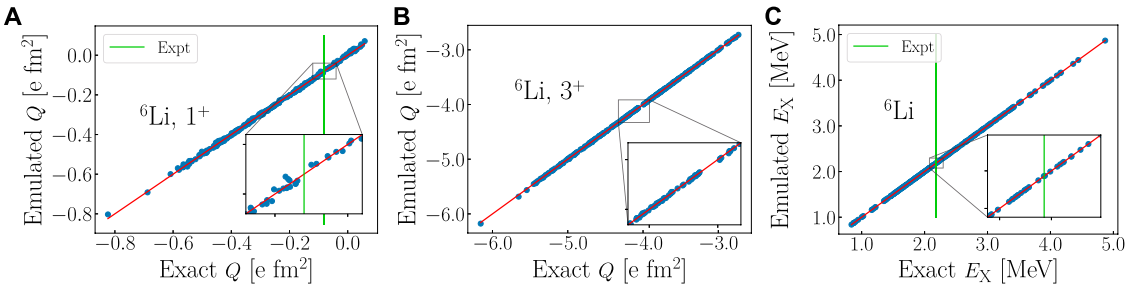

FIGURE 5
Exact vs. SA-EVC observables in ^{6}Li (blue circles) for the quadrupole moment Q of **(A)** the 1^+ ground state and **(B)** the first excited 3^+ state, as well as **(C)** for the excitation energy E_X of the 3^+ state, in $\langle 2_{All}\rangle 8_{13}$ SA model spaces and for $\hbar\Omega$ = 15 MeV. Also shown is the agreement between the exact and emulated values to guide the eye (red line), and experimental results (vertical green line) where available. Insets show 5%-regions surrounding reported experimental data [45] or the NNLO$_{opt}$ result where data is not available [a 50%-region is used for the very small Q in **(A)**].

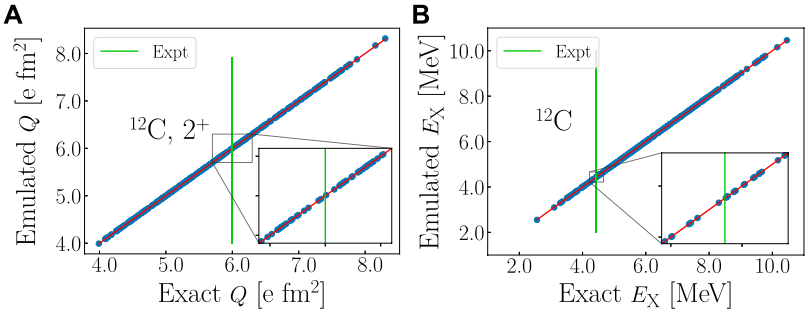

FIGURE 6
The same as in Figure 5 but for **(A)** the quadrupole moment Q and **(B)** the excitation energy of the first 2^+ state in ^{12}C, calculated in 6_3 SA model spaces and for $\hbar\Omega$ = 15 MeV. Insets show 5%-regions surrounding reported experimental data [47].

Conclusion

We have for the first time combined the framework of the SA-NCSM with the EVC procedure into the SA-EVC method for studies of collective and clustering observables. This builds upon earlier SA-NCSM explorations that have shown that an Sp(3,$\mathbb{R}$)-adapted model space selection can successfully capture nuclear collectivity while significantly reducing the sizes of Hamiltonian matrices [8]. Here, we show that excitation energies, point-proton rms radii, electric quadrupole moments and $E2$ transitions in the two lowest-lying states of ^{6}Li and ^{12}C calculated with the specific parameterization NNLO$_{opt}$ for $\hbar\Omega$ = 15 MeV in SA model spaces are in reasonable agreement with those calculated in the corresponding N_{max} complete model space (or equally, to NCSM outcomes). We also show that these observables are converged with N_{max} for the SA selections under consideration.

Further, we demonstrate that SA-EVC emulators trained on SA model spaces are capable of accurately predicting such observables as the LECs are varied, while further reducing the dimensions of operator matrices by an additional 2-3 orders of magnitude. Combined with the initial reduction provided by the SA-NCSM, the emulator matrices have a dimension as much as 10^{-5} times smaller than the corresponding N_{max} complete model spaces. They are small enough to perform linear algebra operations using a single CPU thread on a standard laptop without difficulty. Moreover, the SA-EVC approach will be critical for nuclei beyond the lightest systems; thus, e.g. in ^{20}Ne, the complete N_{max} = 8 model space has dimension of 1.52×10^{11}, while the *ab initio* SA-NCSM solutions are achieved when using 112 million basis states for $J^\pi = 0^+, 2^+, 4^+$. This can be further reduced to emulators of dimension 10^2 especially given the predominance of a single symplectic irrep in the ground-state rotational band of this nucleus. Comparing the emulator results to exact calculations performed in the same SA spaces, we find that the average relative errors are typically 10^{-4}. A larger error ($\sim 10^{-2}$) is found for the quadrupole moment of the ^{6}Li ground state, which is highly sensitive to the L = 2 admixture and hence to the underlying nuclear force, as discussed in the text. A future study that utilizes larger training sets may provide further insight.

In addition to validating the SA-EVC procedure, we show that the symmetry patterns and clustering features in the emulator training wave functions do not respond strongly to variations in the LECs. Across all of the training wave functions, there is a single nuclear shape (approximate symplectic symmetry) that accounts for 81%–94% of the total probability. Furthermore, the dominance of important SU(3) configurations is preserved from one training wave function to

another. Projecting the training wave functions for ^{6}Li onto the $\alpha + d$ system, we find that the likelihood of cluster formation in both the $^3S_1$- and $^3D_3$-wave channels is largely unaffected by the choice of LECs. Spectroscopic factors, ANCs and α-widths extracted from the cluster wave functions all vary within relatively narrow ranges around their average values, ranges that track reasonably well with the 10% variation of the LECs. This suggests that the part of the nuclear potential that is independent of the LECs and is practically the same for all chiral potentials (up to the regularization and related cutoffs employed) provides the dominant features of the wave function, such as Sp(3,$\mathbb{R}$) symmetry patterns and clustering formation, while varying the LECs and associated unresolved short-range interactions has an effect on, e.g., collective quadrupole moments, asymptotic normalization coefficients (ANCs), and alpha partial widths up to a factor of two.

In order to better understand the relationships between collectivity and clustering explored in this study, and how both relate to the underlying nuclear forces, sensitivity analyses are required. As we enter the era of high-precision nuclear physics, this is also an important step towards constructing accurate interactions, with quantified uncertainties. We note that properly accounting for clustering features is important for the *ab initio* modeling of nuclear reactions, and related processes from fusion to fission. The SA-EVC method provides a clear and now verified framework for generating the huge number of chiral parameterizations required for such analyses. Hence, the door is now open to perform *ab initio* calculations with quantified uncertainties that emerge from the interaction and the controlled many-body approximations, from exotic light nuclei up to medium-mass isotopes, as well from spherical to highly enhanced collective and clustering modes.

Data availability statement

The raw data supporting the conclusion of this article will be made available by the authors, without undue reservation.

Author contributions

All authors listed have made a substantial, direct, and intellectual contribution to the work and approved it for publication.

Acknowledgments

We acknowledge invaluable discussions with Jerry P. Draayer, George Rosensteel, David Rowe, and Daniel Langr. This work was supported in part by the U.S. National Science Foundation (PHY-1913728, PHY-2209060), the European Research Council (ERC) under the European Unions Horizon 2020 research and innovation program (Grant agreement No. 758027), the Czech Science Foundation (22-14497S). KSB greatly appreciates the financial support of a research fellowship from the Louisiana Board of Regents. This work benefited from high performance computational resources provided by LSU (www.hpc.lsu.edu), the National Energy Research Scientific Computing Center (NERSC), a U.S. Department of Energy Office of Science User Facility operated under Contract Nos. DE-AC02-05CH11231, as well as the Frontera computing project at the Texas Advanced Computing Center, made possible by National Science Foundation award OAC-1818253.

Conflict of interest

The authors declare that the research was conducted in the absence of any commercial or financial relationships that could be construed as a potential conflict of interest.

Publisher's note

References

1. Johnson CW, Launey KD, Auerbach N, Bacca S, Barrett BR, Brune C, et al. From bound states to the continuum. *J Phys G* (2020) 47:23001. arXiv:1912.00451.

2. van Kolck PF, van Kolck U. Effective field theory for few-nucleon systems. *Annu Rev Nucl Part Sci* (2002) 52:339–96. arXiv:nucl-th/0203055. doi:10.1146/annurev.nucl.52.050102.090637

3. Tews I, Davoudi Z, Ekström A, Holt JD, Becker K, Briceño R, et al. Nuclear forces for precision nuclear physics: A collection of perspectives. *Few-Body Syst* (2022) 63:67. arXiv:2202.01105. doi:10.1007/s00601-022-01749-x

4. Furnstahl RJ, Klco N, Phillips DR, Wesolowski S. Quantifying truncation errors in effective field theory. *Phys Rev C* (2015) 92. doi:10.1103/physrevc.92.024005

5. Hagen A, Hagen G. Global sensitivity analysis of bulk properties of an atomic nucleus. *Phys Rev Lett* (2019) 123:252501. arXiv:1910.02922. doi:10.1103/physrevlett.123.252501

6. Sargsyan GH, Launey KD, Burkey MT, Gallant AT, Scielzo ND, Savard G, et al. Impact of clustering on the Li8 β decay and recoil form factors. *Phys Rev Lett* (2022) 128:202503. arXiv:2107.10389. doi:10.1103/physrevlett.128.202503

7. Stroberg SR, Holt JD, Schwenk A, Simonis J. *Ab initio* limits of atomic nuclei. *Phys Rev Lett* (2021) 126:022501. doi:10.1103/physrevlett.126.022501

8. Dytrych T, Launey KD, Draayer JP, Rowe DJ, Wood JL, Rosensteel G, et al. Physics of nuclei: Key role of an emergent symmetry. *Phys Rev Lett* (2020) 124:042501. arXiv:1810.05757. doi:10.1103/physrevlett.124.042501

9. Launey KD, Mercenne A, Dytrych T. Nuclear dynamics and reactions in the ab initio symmetry-adapted framework. *Annu Rev Nucl Part Sci* (2021) 71:253–77. doi:10.1146/annurev-nucl-102419-033316

10. Launey KD, Dytrych T, Draayer JP. Symmetry-guided large-scale shell-model theory. *Prog Part Nucl Phys* (2016) 89:101–36. arXiv:1612.04298. doi:10.1016/j.ppnp.2016.02.001

11. Frame D, He R, Ipsen I, Lee D, Lee D, Rrapaj E. Eigenvector continuation with subspace learning. *Phys Rev Lett* (2018) 121:032501. arXiv:1711.07090. doi:10.1103/physrevlett.121.032501

12. König S, Ekström A, Hebeler K, Lee D, Schwenk A. Eigenvector continuation as an efficient and accurate emulator for uncertainty quantification. *Phys Lett B* (2020) 810:135814. arXiv:1909.08446. doi:10.1016/j.physletb.2020.135814

13. Djärv T, Ekström A, Forssén C, Johansson HT. Bayesian predictions for $A = 6$ nuclei using eigenvector continuation emulators. *Phys Rev C* (2022) 105. arXiv:2108.13313. doi:10.1103/physrevc.105.014005

14. Rowe DJ. Microscopic theory of the nuclear collective model. *Rep Prog Phys* (1985) 48:1419–80. doi:10.1088/0034-4885/48/10/003

15. Dytrych T, Sviratcheva KD, Bahri C, Draayer JP, Vary JP. Evidence for symplectic symmetry inAb InitioNo-core shell model results for light nuclei. *Phys Rev Lett* (2007) 98:162503. arXiv:0704.1108. doi:10.1103/physrevlett.98.162503

16. Rowe D. The fundamental role of symmetry in nuclear models. *AIP Conf Proc* (2013) 1541:104. arXiv:1304.6115.

17. Navrátil P, Vary JP, Barrett BR. Properties of12Cin theAb InitioNuclear shell model. *Phys Rev Lett* (2000) 84:5728–31. arXiv:nucl-th/0004058. doi:10.1103/physrevlett.84.5728

18. Barrett B, Navrátil P, Vary J. *Ab initio* no core shell model. *Prog Part Nucl Phys* (2013) 69:131–81. doi:10.1016/j.ppnp.2012.10.003

19. Epelbaum E, Nogga A, Glöckle W, Kamada H, Meißner U-G, Witala H. Three-nucleon forces from chiral effective field theory. *Phys Rev C* (2002) 66:064001. arXiv:nucl-th/0208023. doi:10.1103/physrevc.66.064001

20. Entem DR, Machleidt R. Accurate charge-dependent nucleon-nucleon potential at fourth order of chiral perturbation theory. *Phys Rev C* (2003) 68:041001. arXiv:nucl-th/0304018. doi:10.1103/physrevc.68.041001

21. Ekström A, Baardsen G, Forssén C, Hagen G, Hjorth-Jensen M, Jansen GR, et al. Optimized chiral nucleon-nucleon interaction at next-to-next-to-leading order. *Phys Rev Lett* (2013) 110:192502. arXiv:1303.4674. doi:10.1103/physrevlett.110.192502

22. Epelbaum E, Krebs H, Meißner UG. Precision nucleon-nucleon potential at fifth order in the chiral expansion. *Phys Rev Lett* (2015) 115:122301. doi:10.1103/physrevlett.115.122301

23. Schiavilla R, Girlanda L, Gnech A, Kievsky A, Lovato A, Marcucci LE, et al. Two- and three-nucleon contact interactions and groundstate energies of light- and medium-mass nuclei. *Phys Rev C* (2021) 103:054003. arXiv:2102.02327. doi:10.1103/physrevc.103.054003

24. Launey KD, Dytrych T, Sargsyan GH, Baker RB, Draayer JP. Emergent symplectic symmetry in atomic nuclei. *Eur Phys J Spec Top* (2020) 229:2429–41. arXiv:2108.04900. doi:10.1140/epjst/e2020-000178-3

25. Verhaar BJ. A method for the elimination of spurious states in the nuclear harmonic oscillator shell model. *Nucl Phys* (1960) 21:508–25. doi:10.1016/0029-5582(60)90073-0

26. Hecht KT. The use of SU(3) in the elimination of spurious center of mass states. *Nucl Phys A* (1971) 170:34–54. doi:10.1016/0375-9474(71)90681-6

27. Draayer JP, Leschber Y, Park SC, Lopez R. Representations of U(3) in U(N). *Comput Phys Commun* (1989) 56:279–90. doi:10.1016/0010-4655(89)90024-6

28. Langr D, Dytrych T, Launey KD, Draayer JP. Accelerating many-nucleon basis generation for high performance computing enabled *ab initio* nuclear structure studies. *Int J High Perform Comput Appl* (2019) 33:522–33. doi:10.1177/1094342019838314

29. Oberhuber T, Dytrych T, Launey KD, Langr D, Draayer JP. *Discrete and Continuous Dynamical Systems-S* (2021) 14:1111.

30. Dytrych T, Langr D, Draayer JP, Launey KD, Gazda D. SU3lib: A C++ library for accurate computation of wigner and racah coefficients of SU(3). *Comput Phys Commun* (2021) 269:108137. doi:10.1016/j.cpc.2021.108137

31. Mercenne A, Launey K, Dytrych T, Escher J, Quaglioni S, Sargsyan G, et al. Efficacy of the symmetry-adapted basis for *ab initio* nucleon-nucleus interactions for light- and intermediate-mass nuclei. *Comput Phys Commun* (2022) 280:108476. doi:10.1016/j.cpc.2022.108476

32. Akiyama JP, Akiyama Y. Wigner and racah coefficients for SU3. *J Math Phys* (1973) 14:1904–12. doi:10.1063/1.1666267

33. Draayer C, Draayer JP. SU(3) reduced matrix element package. *Comput Phys Commun* (1994) 83:59–94. doi:10.1016/0010-4655(94)90035-3

34. Carvalho J, Le Blanc R, Vassanji M, Rowe D, McGrory J. The symplectic shell-model theory of collective states. *Nucl Phys A* (1986) 452:240–62. doi:10.1016/0375-9474(86)90308-8

35. Baker RB, Launey KD, Bacca S, Dinur NN, Dytrych T. Benchmark calculations of electromagnetic sum rules with a symmetry-adapted basis and hyperspherical harmonics. *Phys Rev C* (2020) 102:014320. arXiv:2003.05865. doi:10.1103/physrevc.102.014320

36. Burrows M, Elster C, Weppner SP, Launey KD, Maris P, Nogga A, et al. *Ab initio* folding potentials for nucleon-nucleus scattering based on no-core shell-model one-body densities. *Phys Rev C* (2019) 99:044603. arXiv:1810.06442. doi:10.1103/physrevc.99.044603

37. Miller S, Ekström A, Hebeler K. Neutron-deuteron scattering cross-sections with chiral *NN* interactions using wave-packet continuum discretization. *Phys Rev C* (2022) 106:024001. arXiv:2201.09600. doi:10.1103/PhysRevC.106.024001

38. Ruotsalainen P, Henderson J, Hackman G, Sargsyan GH, Launey KD, Saxena A, et al. Isospin symmetry in $B(E2)$ values: Coulomb excitation study of ^{21}Mg. *Phys Rev C* (2019) 99:051301. arXiv:1811.00774. doi:10.1103/physrevc.99.051301

39. Dytrych T, Hayes AC, Launey KD, Draayer JP, Maris P, Vary JP, et al. Electron-scattering form factors for ^{6}Li in the *ab initio* symmetry-guided framework. *Phys Rev C* (2015) 91:024326. arXiv:1502.03066. doi:10.1103/physrevc.91.024326

40. Kievsky A, Rosati S, Viviani M, Marcucci LE, Girlanda L. A high-precision variational approach to three- and four-nucleon bound and zero-energy scattering states. *J Phys G: Nucl Part Phys* (2008) 35:063101. arXiv:0805.4688. doi:10.1088/0954-3899/35/6/063101

41. Bacca S, Marchisio MA, Barnea N, Leidemann W, Orlandini G. Crystalline order on a sphere and the generalized thomson problem. *Phys Rev Lett* (2002) 89:052502. doi:10.1103/PhysRevLett.89.185502

42. Carlson J, Gandolfi S, Pederiva F, Pieper SC, Schiavilla R, Schmidt KE, et al. Quantum Monte Carlo methods for nuclear physics. *Rev Mod Phys* (2015) 87:1067–118. arXiv:1412.3081. doi:10.1103/revmodphys.87.1067

43. Dreyfuss AC, Launey KD, Escher JE, Sargsyan GH, Baker RB, Dytrych T, et al. Clustering and α-capture reaction rate from *ab initio* symmetry-adapted descriptions of ^{20}Ne. *Phys Rev C* (2020) 102:044608. arXiv:2006.11208. doi:10.1103/physrevc.102.044608

44. Hupin G, Quaglioni S, Navrátil P. Unified description of ^{6}Li Structure and deuterium-^{4}He Dynamics with chiral two- and three-nucleon forces. *Phys Rev Lett* (2015) 114:212502. doi:10.1103/physrevlett.114.212502

45. Tilley D, Cheves C, Godwin J, Hale G, Hofmann H, Kelley J, et al. Energy levels of light nuclei A=5, 6, 7. *Nucl Phys A* (2002) 708:3–163. doi:10.1016/s0375-9474(02)00597-3

46. Filin AA, Möller D, Baru V, Epelbaum E, Krebs H, Reinert P. High-accuracy calculation of the deuteron charge and quadrupole form factors in chiral effective field theory. *Phys Rev C* (2021) 103:024313. arXiv:2009.08911. doi:10.1103/physrevc.103.024313

47. Kelley J, Purcell J, Sheu C. Energy levels of light nuclei A= 12. *Nucl Phys A* (2017) 968:71–253. doi:10.1016/j.nuclphysa.2017.07.015